BOLLETTINO DI GEOFISICA TEORICA ED APPLICATA VOL. 41, N. 3-4, PP. 193-205; SEP.-DEC. 2000

Age constraints for the evolution of the northern Powell Basin (Antarctica)

F. COREN, E. LODOLO and G. CECCONE

Istituto Nazionale di Oceanografia e di Geofisica Sperimentale - OGS, Trieste, Italy

(Received October 14, 1998; accepted April 24, 2001)

Abstract – The age of the basement of the northern sector of the Powell Basin has been determined, using multichannel seismic reflection profiles, magnetic data, and heat flow measurements. Seismic data show that the northern sector of the Powell Basin is floored by oceanic crust, and presents a well preserved fossil ridge axis. Along three magnetic profiles crossing the ridge axis, oceanic-related magnetic anomalies were identified and interpreted. The analysis indicates that in the northern sector of the Powell Basin, sea floor spreading started at about 28 Ma and almost stopped at approximately 17 Ma. From 17 Ma to about 4 Ma, spreading activity was greatly reduced. The age-depth law has been applied to the oceanic basement, interpreted along a seismic profile, after correction for sediment loading and flexural effects in order to asses its age. Published heat flow data have been reinterpreted, and combined with the magnetic and seismic data. A new map of Chrons for the northern sector of the Powell Basin has been produced, and a tentative sketch for its tectonic development has been outlined.

1. Introduction

The Powell Basin (PB) is located at the north-eastern extremity of the Antarctic Peninsula, (Fig. 1). It is nearly completely surrounded by continental crustal blocks, the only exception being its southern margin where it is connected with the north-western Weddell Sea.

The tectonic development of the PB has been related to the separation of the South Orkney Microcontinent from the Antarctic Peninsula, as a consequence of back-arc processes responsible for the Late Paleogene Scotia Sea opening (King and Barker, 1988; Barker et al., 1991). Recent studies, mostly based on multichannel seismic reflection profiles, have shown that at least the northern sector of the PB is floored by oceanic crust. The extent of the oceanic

Corresponding author: F. Coren; Istituto Nazionale di Oceanografia e di Geofisica Sperimentale - OGS, Borgo Grotta Gigante 42/c, 34010 Sgonico (TS), Italy; phone: +390402140255; fax +39040327307; e-mail: fcoren@ogs.trieste.it

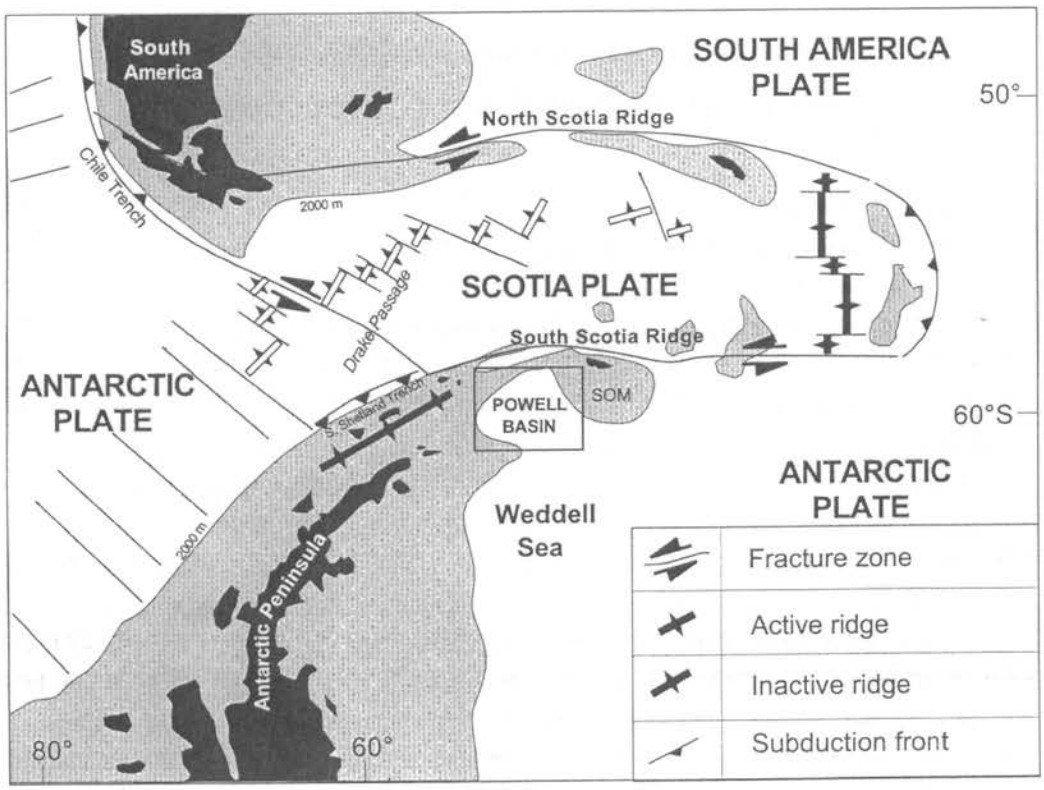

Fig. 1 - Regional tectonic map of the Scotia Sea (after BAS, 1985, modified). Box indicates the study area. SOM=South Orkney Microcontinent.

crust within the PB is however still debated. Rodriguez-Fernandez et al. (1994), and King et al. (1994) consider the whole basin, up to the southern boundary with the Weddell Sea, to be floored by typical oceanic crust, while Coren et al. (1997) confine the accretion of oceanic crust, and the development of the related ridge structure, within an ellipsoidal-shaped area located in the northern sector of the basin. The southern part of the PB, is characterized by rift-related structures (grabens) and consists of highly extended continental crust. The two provinces are not separated by a main tectonic lineation, but they developed coevally as a consequence of the drift of the South Orkney Microcontinent. A confirmation of the different crustal structures of the northern and southern PB is given by interpretation of aerogeophysical data (LaBrecque and Ghidella, 1997). In their Figs. 6 and 8, magnetic anomaly lineations are identified for the PB within an ellipsoidal area located in the northern sector of the basin. These lineations do not continue in the southern part of the PB towards the "Endurance collision zone".

Even though previous studies have revealed some oceanic spreading-related magnetic anomalies in the PB, they are difficult to interpret due to their low amplitude, and the age of the basin has been deduced from the present depth of the top of oceanic layer 2 (King and Barker, 1988), which gives an age between 29 and 23 Ma, and from heat flow measurements (Lawver et al., 1994), which yield an Early Oligocene age for the basin. The sedimentary sequences filling

the basin have been correlated to the main tectonic processes responsible for PB opening (Kavoun and Vinnikovskaya, 1994; Rodriguez-Fernandez et al., 1994), and partially dated using marine magnetic anomalies identified along one profile by Coren et al. (1997). Three different phases in the tectonic development of the PB have been recognized (Coren et al., 1997): an early phase of separation between the Antarctic Peninsula and the South Orkney Microcontinent, which produced stretching and creation of restricted pull-apart basins; oceanic crustal accretion in the northern sector of the basin (Coren et al., 1997; LaBrecque and Ghidella, 1997); a successive clockwise rotation of the South Orkney Microcontinent.

The main aim of this study is to attempt a determination of the age of the oceanic crust in the PB, comparing magnetic anomalies, basement depths and heat flow data. The correct timing of PB evolution is an important element in the frame of the geodynamics of the entire Scotia Arc region.

2. Regional seismic stratigraphy

The seafloor in the basinal area of the PB is remarkably flat and lies at an average depth of 3300 m. The depositional sequences in the PB plain are dominated by hemipelagic and pelagic sediments, with occasional interruptions of thin-bedded turbidities (Lawver et al., 1994), and are relatively constant in thickness. They are characterized on the seismic sections by an upper well-stratified unit with parallel, high-amplitude reflections in the 1.0 - 1.2 s TWT (two-way traveltime) range below the seafloor, and a lower unit with a low-amplitude character. At the center of the basin, these sequences manifest a different character, with a well-stratified appearance throughout the section and strong evidence of current action (King et al., 1994; Rodriguez-Fernandez et al., 1994). Even though the absence of drilling in the PB prevents direct dating of the seismic reflectors, correlations with the drill holes of Leg 113 of the Ocean Drilling Program (ODP) in the South Orkney Microcontinent (Barker and Kennett, 1988) have been attempted (Kavoun and Vinnikovskaya, 1994; Coren et al., 1997).

In the northern part of the PB, three main sedimentary sequences have been recognized (Coren et al., 1997):

- PBS2: covers the majority of the northern PB, except the ridge crest; the thickness varies from 1.0 to 0.1 s TWT. This sequence lies upon unconformity PBBU (PB Breakup Unconformity) at the base, and is topped by the unconformity PBU5A. This depositional event started approximately in the Late Oligocene and concluded in the Early Miocene.
- PBS3: gradually thins and onlaps the ridge axis. This sequence is limited by the unconformity PBU5A at its base and unconformity PBU2 at the top (unconformity U3 of Kavoun and Vinnikovskaya, 1994). It shows near the ridge axis, inner deformations and sediment waves; the deposition of this sequence occurred approximately from the Early Miocene up to the Early Pliocene.
- PBS4: represents the last regional depositional phase recognizable in the PB, and reflects a prevailing undisturbed deposition style. The base of this sequence is the unconformity PBU2. The age of this sequence spans from the Early Pliocene up to the Present.

The multichannel seismic line IT91AW101 has been interpreted where it crosses the ridge axis (Fig. 2); here the sedimentary sequence PBS2 presents an undisturbed sedimentation pattern, with onlap terminations on the ridge structure. The sequence PBS3, which is bounded at the top by the PBU2 unconformity, shows inner deformation in the vicinity of the ridge, and in the proximity of its eastern flank, sediment waves are recognized. The deformations could indicate that ridge activity possibly occurred after the deposition of the PBU2 sequence and during the deposition of the PBS3 unit.

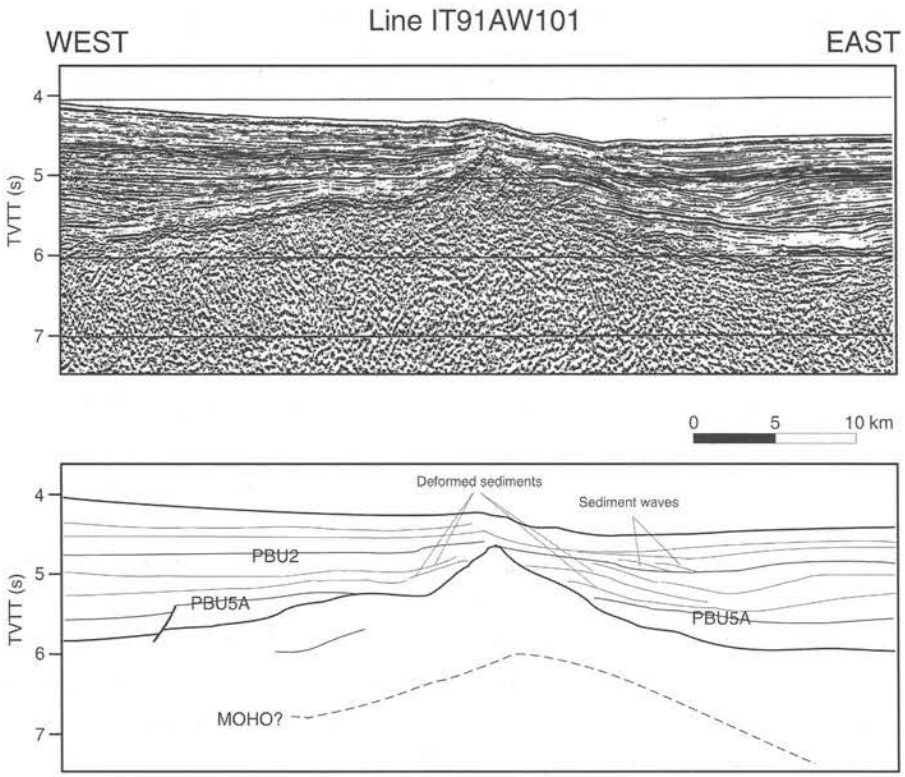

Fig. 2 - Multichannel seismic reflection profile IT91AW101 across the ridge axis in the northern PB (top) and simplified line drawing (bottom). Sedimentary sequences and unconformities are taken from Coren et al. (1997). Location in Fig. 5 (thick line).

3. Magnetic data interpretation

The magnetic profiles used in this study (Fig. 3) were acquired by the R/V OGS-Explora with a proton precession magnetometer (1991 Antarctic Survey, line IT91AW101) and with a proton precession gradiometer (1995 Antarctic Survey, line I95162). The two sensors of the gradiometer were towed at 450 and 300 m from the stern, respectively. The data acquired were processed in order to minimize the effects related to the time variation of the magnetic field. A different processing sequence was applied to the data:

- Line IT91AW101: the profile has been normalized by subtracting the International Geomagnetic Reference Field (IGRF) for the period of investigations (Langel, 1995). In

order to reduce the diurnal variation, a high-pass filter in the frequency domain has been designed and applied to cut frequencies lower than 2 cycles/day. The data noise was then reduced by applying a FFT high-cut filter.

- Line I95162: the gradiometric profile has been processed and the time-dependent component of the magnetic field computed and then subtracted from the data. In order to reduce the data noise, a high-cut filter has been applied. The profile has then been normalized by subtracting the IGRF.

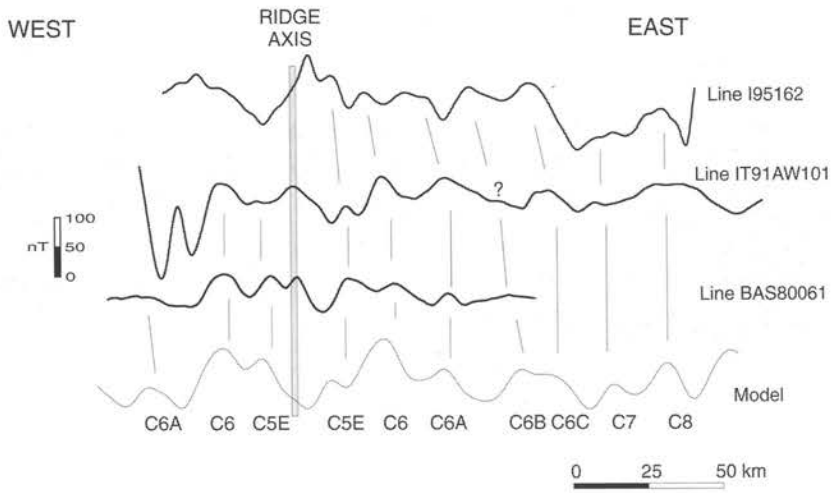

Fig. 3 - Magnetic profiles I95162, IT91AW101, and BAS80061, compared with the magnetic anomaly model computed for a constant spreading velocity of 1.0 mm/yr. See Table 1 for the adopted parameters. Location in Fig. 5.

Previous attempts at identifying magnetic anomalies in the PB (King and Barker, 1988; Lawver et al., 1994) failed, as discussed. This probably depended on three factors: 1 - the anomalies present an anomalous low amplitude in comparison with the normal amplitude shown by spreading-related oceanic anomalies; 2 - because of the low amplitude of the anomalies, the influence of the time-varying component of the magnetic field is relevant and difficult to subtract; 3 - the direction of the previously acquired profiles was not always normal to the mean strike of the supposed magnetized bodies and the extent of the profiles is not sufficient to cover a significant number of anomalies.

The two profiles IT91AW101 and I95162 are useful for the identification of oceanic-related magnetic anomalies in the northern sector of the northern PB. These anomalies have been interpreted by making a comparison with a model which assumes symmetric spreading for the two flanks of the ridge, and projected onto a direction normal to the strike of the ridge axis. The parameters adopted to construct the model are summarized in Table 1.

The profile IT91AW101 crosses the northern part of the spreading center in the PB; the anomaly amplitudes (see Fig. 3) span a few tens of nTs and present the typical shape of spreading-related oceanic magnetic anomalies, even though their amplitude is anomalously low. This profile allows the identification of a complete set of eight sequential Chrons from C5E to C7 (from Late Oligocene to Early Miocene) along the eastern flank of the ridge axis. The Chron

C8 cannot be confidently identified. On the western flank, only two sets of anomalies were identified (Chrons C5E and C6), because the profile, in this part of the basin, does not cross the same extension of oceanic crust. The presence of the Chron C6A has been only inferred.

The profile I95162 (see Fig. 3) crosses both the transitional and oceanic crust that characterize the southern and northern sectors of the PB, respectively (Coren et al., 1997). Similarly, along this profile, the magnetic anomalies are characterized by a few tens of nTs in amplitude, and present a typical oceanic signature. This profile allowed us to identify a set of six magnetic anomalies (from C5E to C7).

In addition to the OGS-Explora data, we consider the British Antarctic Survey profile BAS80061 in Fig. 3 (King et al., 1997). A detailed analysis of the magnetic anomalies along this profile allowed us to compute the spreading velocity for the eastern and western flank of the ridge in the time span 18-21 Ma (Fig. 4). The computed spreading velocities give a value of 14.6 mm/yr (standard deviation of 1.2 Ma) for the eastern flank, and 12.8 mm/yr (standard deviation of 1.3 Ma) for the western flank. For the eastern flank, we computed the linear regression function with the data, integrating the results with those of profile IT95162. In this case, for a time spanning 18 and 26.5 Ma, the linear regression indicates a mean half spreading velocity of 12.8 mm/yr (standard deviation of 0.3 Ma).

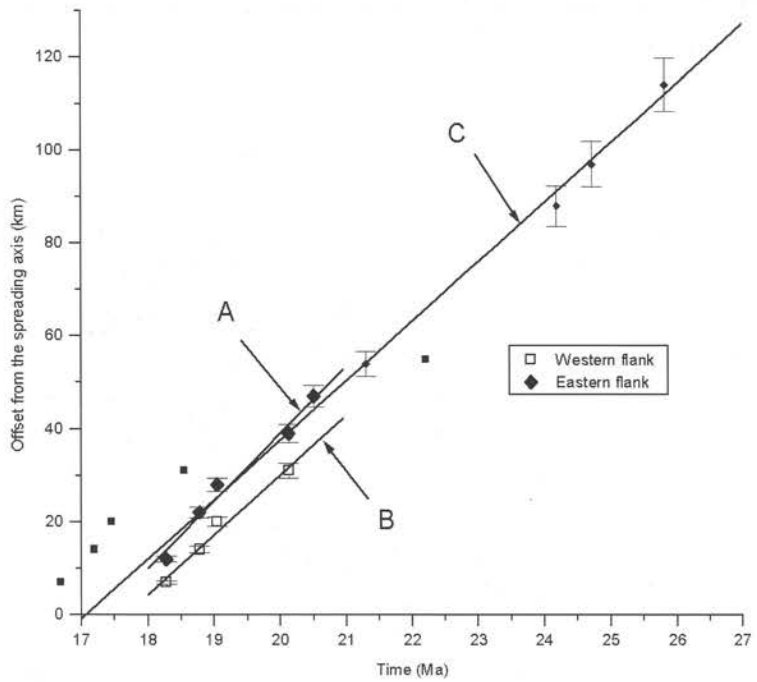

Fig. 4 - Spreading velocities vs. age derived from the interpretation of the magnetic profiles in Fig. 3. The linear regression function computed on the data spans the time interval 16-21 Ma. Line A represents the linear regression of 5 data points of the eastern flank of the ridge (profile BAS80061), where the computed half spreading velocity is 14.6 mm/yr, with a standard deviation of 1.2. Line B represents the linear regression of 4 data points of the eastern flank of the ridge (profile BAS80061), where the computed half spreading velocity is 12.8 mm/yr, with a standard deviation of 1.3. Line C represents the linear regression of 13 data points of both flanks of the ridge (profiles BAS80061 and IT95162), where the computed half spreading velocity is 12.8 mm/yr, with a standard deviation of 0.3.

Table 1 - Parameters adopted for the magnetic model shown in Fig. 3.

Time-scale	Cande and Kent (1995)
Latitude of the model	-60.0° S
Longitude of the model	-52.0° W
Declination	+70.0°
Dip	-70.0°
Strike of the magnetized bodies	+90.0°
Track obliquity	0.0°
Station separation normal to body strike	1 km
Body thickness	0.5 km
Depth to top of ridge (from seismic data)	3.5 km
Susceptibility	0.02 (S.I.)
Spreading rate from -28 to -18 Ma	0.90 cm/yr
Spreading rate from -18 to 18 Ma	0.01 cm/yr
Spreading rate from 18 to 28 Ma	0.90 cm/yr

Combining the results of the magnetic data interpretation, we reconstructed the spatial distribution of the Chrons in the northern part of the PB (Fig. 5), assuming that no discontinuities are present along the flow lines.

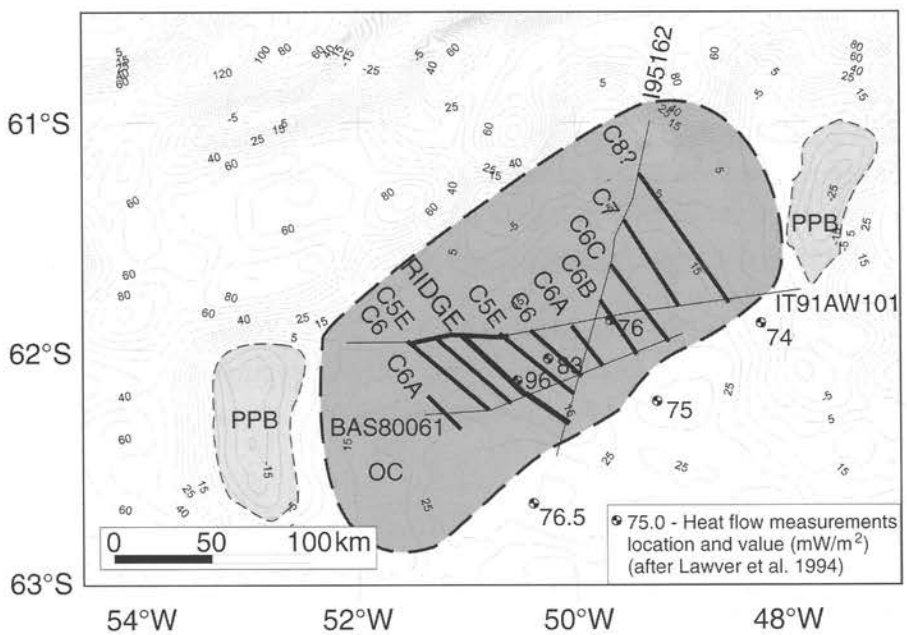

Fig. 5 - Map of the Chrons for the northern PB, derived from the interpretation of the magnetic profiles in Fig. 3. Superimposed are the satellite-derived gravity contours in mGal (Sandwell, 1992), and the heat flow measurements (Lawver et al., 1994). The area of oceanic crust (OC) and the Proto Powell Basins (PPB) are indicated with heavy shading. The part of the seismic profile IT91AW101 shown in Fig. 2 is indicated by the thick line.

4. Flexural decompaction

Theoretical and empirical observations (Davis and Lister, 1974; Parsons and Sclater, 1977) assess the existence of a relationship between the ocean-floor subsidence and the square root of its age. To apply this law, we corrected the ocean basement depth along the multichannel seismic profile IT91AW101 for the sediment and water load, adopting the following procedure: the sediment load correction was computed considering the changes in density with depth (d_z) due to compaction. Since direct measurements from drill holes are not available, we assumed a compaction curve derived from the following porosity-depth equation (Nagumo, 1965):

$$d_z = d_m - (d_m - d_p)\, p_0 \exp(-C\, z)$$

where z is the depth (km), dp (Mg/m^3) and dm (Mg/m^3) are the density of the porous media and of the matrix respectively, p_0 is the porosity and C is an empirical factor related to the compressibility.

Considering the expected pelagic and hemipelagic lithology for the sediment in the basin (Lawver et al., 1994), we assumed:

$C = 0.5$ km^{-1},

$d_m = 2.7$ Mg/m^3 according to the mean values recorded at ODP sites 694-697 (Barker et al., 1988),

$d_p = 1.03$ (Mg/m^3 assuming water as the principal fluid present in the sediment pores.

The simple mass balance model, assuming an Airy model of isostasy (elastic thickness of the crust, $Te = 0$ km), has been enhanced by considering the elastic rebound of the oceanic crust. This further computation was introduced because part of the sedimentary column deposited over an already consolidated crust ($Te \neq 0$ km) of a no longer developing basin, as indicated by the presence of a fossil ridge axis (Coren et al., 1997). We introduced an elastic thickness ($Te = 5$ km) for the removal of the sequence deposited after spreading ceased, considering the relationship between Te and the relatively young age of the crust expected at the time of loading (Watts, 1978). The basement depth, before and after correction, is shown in Fig. 6. The empirical age-depth relationship that estimates the age for any given depth of the oceanic basement (Parsons and Sclater, 1977), is:

$$d(t) = 2500 + 350(t^{1/2})$$

where d is the depth (m) and t the age (Ma). The computation gives an age of about 28.5 Ma for the beginning of the oceanic sea floor spreading (see Fig. 6, arrow A); the depth at the base of the ridge indicates an age of 16 Ma (see Fig. 6, arrow B); the top of the ridge, lying at the computed depth of 3150 m, can be tentatively associated to an age of 4 Ma (see Fig. 6, arrow C).

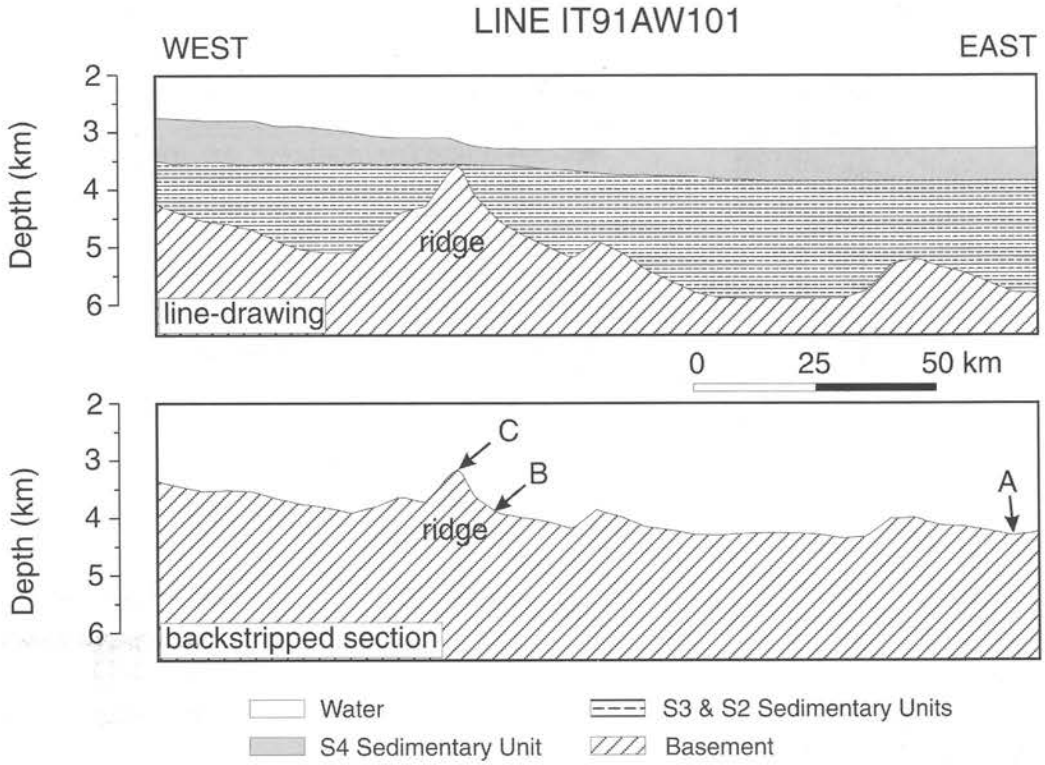

Fig. 6 - Results of the flexural decompaction computed along the line IT91AW101 (see Fig. 5 for location). The upper section represents the digitized seismic profile of Fig. 2, after depth conversion. The depth conversion has been computed adopting the velocity functions derived from common-velocity-stack analysis. The lower section shows the basement profile, after flexural decompaction correction. The correction considers both the effects of the isostatic rebound due to the removal of the water load and the two sedimentary bodies, and the flexural effects of the elastic response of the crust. The arrow marked with an A indicates the oldest oceanic crust, B the base of the ridge, C the top of the ridge.

5. Thermal flow data

Lawver et al. (1994) published a set of heat flow data in the PB (see Fig. 5). These measurements represent the only thermal data available for the area. In the northern part of the basin, three data points are aligned normally to the ridge; one of the points is located in proximity of the top of the fossil ridge axis. The other two data points allowed us to link the heat flow data and the age of the oceanic crust as inferred from the magnetic anomalies. We compared the heat flow data with the thermal flux vs. age values reported by Stein and Stein (1994) for oceanic crust (Fig. 7). We have to point out that the heat flow data of Fig. 5 (Lawver et al., 1994) are not corrected for the sediment thickness; this is because the thickness of sediments beneath the measured points was not available. Application of a sediment-correction would increase the observed heat flow values, which (contrary to what was stated by Lawver et al., 1994) yields a younger age with respect to the postulated Early Oligocene (Lawver et al., 1994). The PB heat flow uncorrected data fit the average of the observed data of Stein and Stein (1994).

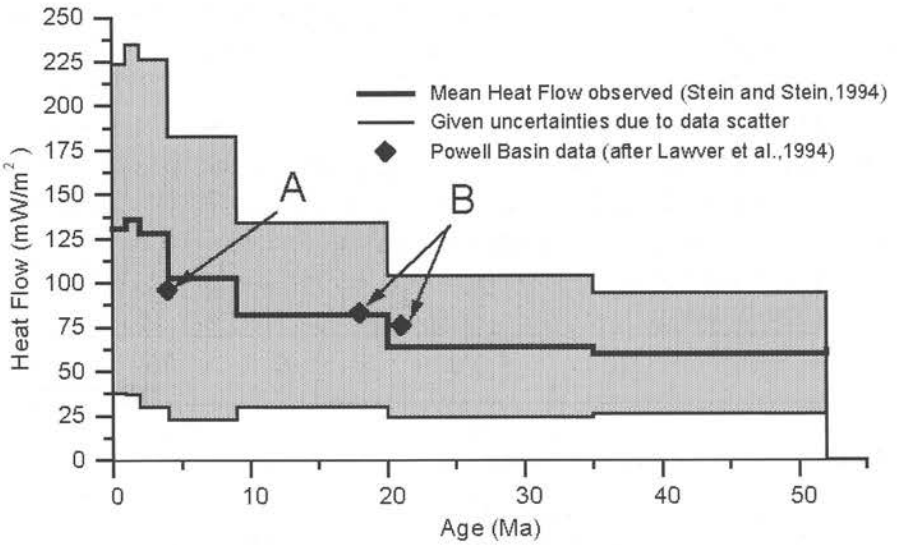

Fig. 7 - Heat flow vs. age plot for the northern PB. The ages of the crust related to heat flow measurements (Lawver et al., 1994), have been derived from the results of the present work. The age of the point indicated by arrow A has been inferred from the flexural decompaction computation. The age of the two points indicated by arrow B has been inferred by magnetic anomaly interpretation. The plot shows a good agreement with the values reported by Stein and Stein (1994) for oceanic crust.

6. Discussion

In addition to seismic data (Coren et al., 1997), the continuity of the ridge structure in the northern part of the PB is suggested by both satellite-derived gravity map (see Fig. 5) and magnetic lineaments. In this sector of the PB LaBrecque and Ghidella (1997) recognized magnetic lineations from aeromagnetic data (see their Figs. 6 and 8). King et al. (1997) identified the volcanic features in the central area of the PB which have been related to extrusive centers of possibly Cenozoic age. All these observations suggest the presence of a well developed ridge structure in the northern PB associated with a relative gravimetric low. The relative gravimetric low may be due to the presence of a thermal high (Lawver et al., 1994), located along the axis of the extrusive center.

The results of the magnetic anomaly interpretation and the age-depth relationship, are consistent within a tolerance of approximately ±1.5 Ma. Spreading occurred before 26 Ma, according to the magnetic interpretation, and before 28.5 Ma, according to the age-depth law. The base of the ridge axis (indicated by arrow B in Fig. 6), has been dated 18 Ma by magnetic interpretation, and 16 Ma by the age-depth relationship. A thick sedimentary sequence onlapping the flanks of the ridge testifies that the ridge structure developed in alternate phases, even after 16 Ma. This is shown by the deformation of the sedimentary sequences deposited before the PBU2 (Kavoun and Vinnikovskaya, 1994; Coren et al., 1997), which represents the base of the first underformed sequence. To date the latest event of the reactivation process, we adopted the age-depth relationship. This analysis indicates an age of about 4 Ma for the top of the ridge, a value which is consistent with heat flow data. Depth and heat flow data may be

misleading for the ridge-crest age determination, but reactivation is supported by the negative gravity anomaly (about 20 mGal) associated with the spreading axis (Kavoun and Vinnikovskaya, 1994). In their gravity model of Fig. 6.14, they consider a density of 2.2 Mg/m^3 for the central ridge block, a value that can be related to a recent emplacement of magmatic material. The same consideration can be made for the free-air gravity anomaly map, which presents a relative low along the ridge, associated with the contour line of 15 mGal.

The sequence of tectonic events that occurred in the northern PB, as interpreted by combining the geophysical evidence already discussed, is given in Table 2.

Table 2 - Comparison between the age of the basement computed by magnetic anomaly interpretation and the age-depth law.

Method	**Oldest oceanic crust** (arrow A of Fig. 6)		**Base of the ridge** (arrow B of Fig. 6)		**Top of the ridge** (arrow C of Fig. 6)
magnetic anomaly interpretation	26.5 Ma	mean value	17.0 Ma	mean value	
oceanic crust elevation vs. age	28.5 Ma	27.5 ± 1Ma	16.5 Ma	17.3 ± 1Ma	4.0 Ma

The evolutionary history of the PB, since the Oligocene, can be summarized in the following two phases (Coren et al., 1997):

1. Evolution of the oceanic basement by sea floor spreading in the Oligocene, which is consistent with the eastward drift of the South Orkney Microcontinent; this phase stopped in the Early Miocene.
2. Later development of the ridge structure with reactivation of magmatic and/or spreading processes, which stopped in the Miocene; this phase is related to the clockwise rotation of the South Orkney Microcontinent

7. Conclusions

Available seismic, magnetic, and satellite-derived gravity data confirm that the northern part of the PB is floored by oceanic crust, and a well preserved ridge structure is present in the center of the basin. The magnetic anomaly distribution in the northern PB indicates that sea floor spreading started at 26 Ma approximately (Chron C8) and stopped at 18 Ma (Chron C5E). There is evidence of an asymmetric distribution of the spreading velocities for the two flanks of the ridge. The spreading velocity of the western flank of the ridge was 15% slower than of the eastern flank. This spreading was driven by a faint rotation of the South Orkney Microcontinent, as inferred from the fan-shaped distribution of the Chrons.

The age-depth relationship, after sediment decompaction applied, is in good agreement with the magnetic results. The base of the ridge axis structure is fixed at 18 Ma (from the magnetic interpretation). This indicates that in the 4-18 Ma period, the spreading velocity was extremely

low or that there was a quiescent period, followed by a reactivation or a single episode of volcanism. We are not able to indicate which of the hypotheses is the most reliable given the existing data. Available heat flow data agree with the age inferred from magnetic anomaly identifications, and support the hypothesis that the last ridge related activity stopped at about 4-5 Ma, as computed by application of the age-depth relationship.

Acknowledgements. Funds for this study were provided by the Italian Programma Nazionale di Ricerche in Antartide (PNRA).

References

Barker P. F., Dalziel I. W. D. and Storey B. C.; 1991. *Tectonic development of the Scotia Arc region.* In: Tingley R.J. (ed): The Geology of Antarctica, Oxford Science Publications, 215-248.

Barker P. F. and Kennett J. P.; 1988. *Proceedings ODP Program*, Init. Rep., **113**, College Station, TX, 785 pp.

BAS; 1985: Tectonic Map of the Scotia Arc, Cambridge, British Antarctic Survey.

Cande S. C. and Kent D. V.; 1995. *Revised calibration of the geomagnetic polarity time scale for the Late Cretaceous and Cenozoic.* Journal of Geophysical Research, **100**, 6093-6095.

Coren F., Ceccone G., Lodolo E., Zanolla C., Zitellini N., Bonazzi C. and Centonze J.; 1997. *Morphology, seismic structure, and tectonic development of the Powell Basin, Antarctica.* Journal of Geological Society, London, **154**, 849-862.

Davis E. E. and Lister C. R. B.; 1974. *Fundamentals of ridge crest topography. Earth and Planetary Sciences Letters*, **21**, 405-417.

Kavoun M. and Vinnikovskaya O.; 1994. *Seismic stratigraphy and tectonics of the northwestern Weddell Sea (Antarctica) inferred from marine geophysical surveys.* Tectonophysics, **240**, 299-341.

King E. C. and Barker P. F.; 1988. *The margins of the South Orkney Microcontinents.* Journal of the Geological Society of London, **145**, 317-331.

King E. C., Leitchenkov G., Galindo-Zaldivar J., Maldonado A. and Lodolo E.; 1997. *Crustal Structure and Sedimentation in Powell.* In: Barker P. F., Cooper A. K. (eds): Geology and Seismic Stratigraphy of the Antarctic Margin, Part 2, Antarctic Research Series, Vol. 71, pp. 75-93.

King E. C., Leitchenkov G., Galindo-Zaldivar J. and Maldonado A.; 1994. *Basement Distribution in Powell Basin: Understanding the Tectonic Controls on Sedimentation.* Terra Antartica, **1**, 307-308.

LaBrecque J. L. and Ghidella M. E.; 1997. *Bathymetry, depth to magnetic basement and sediment thickness estimate from aerogeophysical data over the western Weddell Basin.* Journal of Geophysical Research, **102**, B4, 7929-7945.

Langel R .A.; 1995. *International Geomagnetic Reference Field, 1991 Revision.* EOS Trans. AGU, 76: 184.

Lawver L. A., Williams T. and Sloan B.; 1994. *Seismic stratigraphy and heat flow of Powell Basin.* Terra Antartica, **1**, 309-310.

Nagumo S.; 1965. *Compaction of Sedimentary Rock. A Consideration by the Theory of Porous Media.* Bulletin of Earthquake Research Institute, Tokyo, **43**, 339-348.

Parsons B. and Sclater J. G.; 1977. *An analysis of the variation of ocean floor bathymetry and heat flow with age.* Journal of Geophysical Research, **82**, 803-827.

Rodriguez-Fernandez J., Balanya J. C., Galindo-Zaldivar J. and Maldonado A.; 1994. *Margin styles of Powell Basin and their tectonic implications (NE Antarctic Peninsula).* Terra Antartica, **1**, 315-316.

Sandwell D. T.; 1992. *Antarctic marine gravity field from high-density satellite altimetry.* Geophysical Journal International, **109**, 437-448.

Sclater J. C., Jaupart C. and Galson D.; 1980. *The Heat Flow Through Oceanic and Continental Crust and the Heat Loss of the Earth.* Reviews of Geophysics and Space Physics, **18**, 269-311.

Stein C. A. and Stein S.; 1994. *Constraints on hydrothermal heat flux through the oceanic lithosphere from global heat flow.* Journal of Geophysical Research, **99**, 3081-3095.

Watts A. B.; 1978. *An Analysis of Isostasy in the World's Oceans.* Journal of Geophysical Research, **83**, 5989-6004.